Journal of Materials Chemistry A

Morphology Engineering of Protein Fabrics for Advanced and Sustainable Filtration

Journal:	*Journal of Materials Chemistry A*
Manuscript ID	TA-ART-09-2018-008717.R1
Article Type:	Paper
Date Submitted by the Author:	11-Oct-2018
Complete List of Authors:	Fan, Xin; Huazhong Agriculture University Wang, Yu; Washington State University, School of Mechanical and Materials Engineering Zheng, Min; Washington State University College of Business, Mechanical and Materials Engineering Dunne, Francis; washington state university Liu, Tian; Washington State University, College of Materials Science and Engineering Fu, Xuewei; Washington State University, School of Mechanical and Materials Engineering Kong, Lushi; Beijing University of Chemical Technology Pan, S.-Y.; Huazhong Agriculture University Zhong, Katie; Washington State University, Mechanical and Materials Engineering

Journal of Materials Chemistry A

ARTICLE

Morphology Engineering of Protein Fabrics for Advanced and Sustainable Filtration

Received 00th January 20xx,
Accepted 00th January 20xx

DOI: 10.1039/x0xx00000x

www.rsc.org/

Xin Fan,[a,b,c] Yu Wang,*[b] Min Zheng,[b] Francis Dunne,[b] Tian Liu,[b] Xuewei Fu,[b] Lushi Kong,[d] Siyi Pan*[a,c] and Wei-Hong Zhong*[b]

High removal efficiency, low flow resistance, high filtration capacity of pollutants and the capability of removing different types of pollutants are critical for advanced air-filters. However, it has been very challenging to simultaneously realize these performances for traditional filtering materials. Here, we report a study on development of new strategy for fabrication of multi-functional protein fabrics with novel ribbon morphology and cotton-candy-like structures to address the above challenge. In particular, a metastable solution of zein protein in a mixture solvent is proposed for the first time to fabricate the ribbon-like fibre with self-curving behaviour. This self-curved zein fabric has multiple significant contributions to filtration. Firstly, the ribbon morphology notably enhances the trapping capability for especially sub-micron particulate pollutants. Secondly, the self-curving feature of the fibres generates cotton-candy-like loose structures and elastic property for the fabric, which significantly reduces the flow resistance. As a result, the filtration performances have been simultaneously improved, including enhanced capture efficiency, filtration capacity and stability of air pressure drop, as well as the reduced airflow resistance, as compared with traditional fabrics with rod-shaped fibres. This study does not only provide a new electrospinning strategy for fabrication of functional ribbon-like fibres,

[a] *College of Food Science and Technology, Huazhong Agricultural University, No. 1 Shizishan Road, Wuhan, Hubei, 430070, PR China*
[b] *School of Mechanical and Materials Engineering, Washington State University, 100 Dairy Road, Pullman, WA, 99164, USA*
[c] *Key Laboratory of Environment Correlative Dietology (Huazhong Agricultural University), Ministry of Education, No. 1 Shizishan Road, Wuhan, Hubei, 430070, PR China*
[d] *College of Materials Science and Engineering, Beijing University of Chemical Technology, North Third Ring Road, Beijing, 100029, PR China*
† Electronic Supplementary Information (ESI) available. See DOI: 10.1039/x0xx00000x

but also brings about a guideline for the design of advanced fabrics for various filtration applications.

1. Introduction

Air pollution brings about many issues to public health and environment because of the unpredictable and instable compositions of the pollutants that are usually harmful to most of the living organism.[1-3] There are two primary characteristics about air pollutants. Firstly, the compositions of pollutants are unpredictable, constantly changeable and complicated. Air pollutants are usually comprised of particulate matter (PM) of various sizes, chemical gas of different species, micro-organisms,[4] and so on. PM in the polluted air has complicated morphology and compositions including primary emission and secondary formation. The primary emission contains nitrates (NO_3^-),[5] sulphate (SO_2^{2-} and SO_4^{2-}),[5] mineral dust,[6] black carbon,[4] etc. from different sources, such as vehicular and industry emission,[7, 8] biomass burning.[9] In addition, the secondary aerosols are another major source of pollutant particles in terms of their number concentrations.[10, 11] Recently, Wang et. al. found that sulfuric acid and amines played a critical role in the formation of PM through a new particle formation process.[12] This study indicates that the new particle formation process is a result of the formation of large concentrations of new atmospheric particles, and there are complicated interactions among different pollutants, on which people have very limited knowledge or less awareness thus far. Based on the particulate size, PM can be categorized into different levels, such as $PM_{2.5}$ that refers to the particulate matter with the size below 2.5 μm.[9] PM is one of the primary pollutants in polluted air due to its serious impacts on the health of people and wild lives, local climate, and ecosystems.[13-15] $PM_{2.5}$ is particularly harmful since it can penetrate human bronchi and lungs due to the small particle size.[9] Besides, $PM_{2.5}$ has a long lifetime in the air from days to weeks, whereas, the lifetime of $PM_{2.5-10}$ in the air is much shorter (only from minutes to hours) and $PM_{2.5-10}$ has a very limited traveling distance.[5] Secondly, another characteristic of air pollutants is that the pollutant concentrations or polluted level can change remarkably from place to place, or from season to season. For example, there is usually heavy air pollution in the place with dense manufacturing industries and vehicles.[9] Similarly, the air pollution issues become more serious in the winter time due to temperature effects and seasonal source of air pollution.[16] Considering the above

characteristics about air pollutants, the design of air-filters has to incorporate several important properties simultaneously. These properties include multi-functionality for removing different types of pollutants, high removal efficiency for different pollutants, high filtration capacity of removing the pollutants in highly or lightly polluted air with a sufficient serving lifetime, and importantly, low airflow resistance to reduce the energy-consuming and increase the work efficiency of the filtration system.

However, it is very challenging to simultaneously realize these properties in an air-filter mat made of one active material for multiple reasons. Firstly, the filtration materials are usually functionally limited. In other words, one type of filtration material can only remove very few types of pollutants,[17, 18] which indicates that the filter has to include different types of filtration materials in order to removal different pollutants (e.g. PM and toxic gases). For example, synthetic polymers are the most popular filtration materials used for air-filters and they are fabricated into different configurations, such as porous membrane filters and fibrous filters.[18] Compared with porous membrane filters (only based on size sieving mechanism), the fibrous filters have multi-filtration mechanisms, such as sieving, inertial impaction, interception and diffusion[4, 5], which usually give rise to a high removal efficiency for air pollutants.[19] However, their function is often limited by PM filtration. Recently, nanofibers by electrospinning of different polymers, such as polypropylene (PP),[9, 20] nylon,[21] polyacrylonitrile (PAN),[5, 22] chitosan,[23] polyvinyl alcohol (PVA),[9] polyvinylpyrrolidone (PVP),[9, 23] polystyrene (PS)[9, 23] and polyimide (PI),[5] have attracted tremendous attention for air filtration. Although these nanofibers showed much improved filtration performance primarily as a result of the high surface area of the nanofibers, their filtration performance is still limited, especially for small particles.[6, 18, 24] Secondly, the trade-offs among filtration efficiency, airflow resistance and filtration capacity represents another challenge for current filtration materials.[3] For examples, to reduce flow resistance, Cui et. al. reported a transparent air-filter made of a very thin layer of PAN nanofibers.[9] Although they achieved high removal efficiency and low flow resistance, the filtration capacity is a big concern since there was only a very small amount of active material. A composite air-filter with a hierarchical structure was reported to

achieve low flow resistance and high loadings of active filtration materials or high filtration capacity, the filtration efficiency for small pollutants is sacrificed.[25] Recently, natural protein nano-fabrics have been demonstrated to have potential of achieving multi-functional filtration capabilities[4, 6, 18, 24, 26, 27] However, similar to other Nano fabrics, it remains problematic to simultaneously achieve low airflow resistance and high filtration capacity for the protein fabrics fabricated by electrospinning. This is mainly due to the fact that electrospinning tends to form compact fabrics with uncontrollable porous structures under the effects of the strong electrical field. Therefore, strategies for addressing this challenging issue for the fabrics fabricated by electrospinning are in critical need for the development of multi-functional and high-performance protein-based air-filters.

In this study, inspired by the loose structures of cotton-candy, we aim to fabricate a multi-functional protein fabric with a novel ribbon morphology to address the above challenge. We found that the solvent for the protein solution plays a pivotal role in controlling the morphology and thus the mechanical properties of the protein fibres. Via control of solvents, we successfully achieved the desirable structures of protein fabrics prepared by electrospinning. As illustrated in Fig. 1a, when zein protein is dissolved in acetic acid (AA)/deionized water (DI) mixture solvent and a stable protein solution is present, one can easily fabricate straight rod-zein fibres and finally resulted in compact fabrics with a sheet structure. There are mainly two drawbacks about this type of fabric. Firstly, the airflow resistance will be very high especially when thick fabric is desired. Secondly, the rod morphology can weaken the trapping capability as illustrated in Fig. 1a. For example, part of small air pollutants may escape from the rod fibre after their impact on the fibre surface, or easily bypasses the rod fibre along with the airflow. In this case, the trapping of small pollutants is highly dependent on the attractive force among the pollutants and the fibre surface. Instead of stable solution as traditionally used for electrospinning, we developed a metastable zein solution, for the first time, in a mixture solvent of acetone/butanol/DI (weight ratio of 2:1:1) to fabricate the desired ribbon-like fibre with self-curving behaviour to control the porous structures of the final fabric. As shown in Fig. 1b, compared to the traditional rod-zein

fibre, the self-curved ribbon zein fabric has multiple significant advantages for filtration. Firstly, the self-curving behaviour of the fibres generates cotton-candy-like loose structures and elastic property for the fabric, which can significantly reduce the flow resistance. Secondly, the ribbon morphology notably enhances the capability of trapping pollutants especially for small particulate pollutants. This ribbon-zein fabric can enhance trapping capability via synergistic effects of enhanced blocking effect and attractive interactions from the functional groups on the surface as illustrated in Fig. 1b**.** In specific, there are plenty of functional groups on the fibre surface to generate strong interactions with air pollutants. At the same time, when the PM particles or chemical gaseous molecules hit on the ribbon-like fibres, there is much less chance for them to escape as the ribbon structure can generate "multiple blocking effects". Combining these two effects, the small pollutants can be easily trapped by the ribbon-like fibres. Due to the above advantages, the removing efficiency, both the air permeability and the filtration capacity can be significantly improved as compared with traditional rod fabrics.

2. Result and discussion

2.1 Zein-protein denaturation

To analyze the denaturation of zein in two kinds of mixture solvents, FTIR, particle size and transmittance studies were performed. Fig. 2a shows the FTIR spectrum of the pristine zein powders, rod-zein and ribbon-zein fabrics. The three samples show several important absorption characteristic peaks at about 3295 cm^{-1} (-OH bands), 2949 cm^{-1} (-CH_2CH), 1654 (-C=O bands), 1541 cm^{-1} (amide II -NH bands) and 1257 cm^{-1} (amide I -NH bending).[28, 29] For the zein fabrics prepared by the stable and metastable solution, the main absorption peaks in the FTIR spectrum are similar with each other and no notable change can be found if compared with that for the pristine zein powders. This result shows that the solvents in these two cases make trifiling impact on the primary structure of zein protein and there was no chemical reaction between the solvent and the zein protein. In Fig. 2b, the dynamic light scattering result indicates that the particle size of denatured zein in the stable solution is larger than that in metastable solution. This is probably because the zein protein in the metastable solution is denatured more completely and

the protein chains become more unfolding. The transmittance of the stable and metastable zein solutions with the same solid concentrations (25 wt%) in the range of 200 - 1100 nm wavelength is shown in Fig. 2c. In specific, the stable zein solution shows transmittance less than 1% in the UV and visible regions, and less than 8% in the IR region (600-1100 nm). For the metastable zein solution, it also showed a very low transmittance in the UV region. This UV block phenomenon is mainly attributed to the UV-absorption ability of the aromatic amino acid residues in the zein protein.[30] However, in the visible and IR regions, the metastable zein solution displays a much higher transmittance than stable zein solution as shown in Fig. 2c. The values reach about 7% and 25% for the visible and IR regions, respectively. Fig. 2d and e are the digital photos of the two solutions. One can find that the metastable zein solution is more transparent than the stable zein solution, which is consistent with the above transmittance spectra result.

To understand the above differences in protein denaturation and solution structures, the roles of solvent are further analysed in Fig. 2f and g. It is well known that proteins possess four levels of structure, including primary, secondary, tertiary and quaternary structures.[31] The tertiary structure including salt bridges, hydrogen bonds and disulphide bonds, are very important factors determining the conformation of protein. The denaturation process is usually the process of destroying the native secondary, tertiary and quaternary structures, which helps to expose the functional groups.[32, 33] Acids and alcohol have been reported as effective solvent to destroy secondary and tertiary structures.[34] For the stable solution in AA/DI mixture solvent, the addition of acetic acid (AA) may destroy the salt bridges of protein, as illustrated in Fig. 2f. For the metastable solution, the hydrogen bonds and disulphide bonds of tertiary structure may be broken by butanol and acetone,[34] as illustrated in Fig. 2g. With the help of acetone and butanol solvent, the zein proteins become more unfolded and denatured as compared with the zein in the AA/DI system. The solvent not only generates the above difference in protein denaturation, but also significantly affects the structure evolution during evaporation. These two factors together notably change the structure/morphology of the zein fibres as introduced below.

2.2 Electrospun fabrics from the two protein-sovlent systems

The above results show that the solvent makes a big difference in the denaturation or dissolving of the zein protein. More significantly, we find that it finally controls the morphology of the fibres and the fabric. The results about the fabric structures are shown in Fig. 3. One can clearly find the big difference in morphology from the SEM and TEM images. In specific, as shown in Fig. 3a–f, and Fig. ESI1 †, the stable zein solution in AA/DI solvent gives rise to traditional nanofibers with straight rod morphology, which finally results in a paper-like compact fabric. In contrast, as shown in Fig. 3g–l, the fibre morphology changes remarkably for the metastable zein solution in Acetone/Butanol/DI. Firstly, instead of rod fibres, a novel ribbon-like fibre is achieved (see Fig. 3h and i, and Fig. ESI2†). Secondly, the ribbon-like fibres are self-curved as shown in Fig. 3g and j, resulting a cotton-candy-like loose fabric (for more SEM images, see Fig. ESI2†). This morphology change from straight rod fibre to self-curved ribbon-like fibre finally makes a big difference in the porous structures of the resultant fabrics. As shown by Fig. 3 e and f, the thickness of the rod-zein fabric is about only 8 μm with a fibre areal density of ca. 12 g m^{-2}. With a similar fibre areal density, the thickness of the ribbon-zein fabric is ca. 130 μm, showing much looser structures (see Fig. 3k and i). As a result, the porosity of the rod-zein fabric is ca. 32%, only around one third of the ribbon-zein fabric (ca. 83%), as shown in **Table ESI1**†.

The self-curved ribbon morphology will significantly benefit air filtration as will be discussed later. The diameter, width and thickness of fibre were statistically analysed by Image-Pro Plus. The results are summarized in Fig. 3m and n. As displayed, the mean diameter of the rod-zein fibre is ca. 0.12 μm; while the width and thickness of the ribbon-zein fibre are 2.79 μm and 0.80 μm, respectively. The big difference in morphology further changes the mechanical properties for the two kinds of fabrics. As shown in Fig. 3 o, the tensile test results reveal that the mechanical strength of the ribbon-zein fabric is much higher than rod-zein fabric. The maximum stresses for the rod-zein fabric and ribbon-zein fabric are ca. 1.00 MPa and 0.65 MPa, respectively. This is probably due to the entanglement effects from curved fibres and ribbon morphology. Moreover, the self-curved

ribbon-like fibres are more elastic than straight rod fibre as shown in Fig. 3o. There is an elastic deformation zone as indicated by the strain from 18% to 23%. This is interesting as proteins are generally brittle polymers. The self-curving ribbon-like fibre may generate spring-like mechanical properties regardless of its brittleness. Moreover, as mentioned above, the porosity of the ribbon-zein fabric is ca. 83%, about triple of the rod-zein fabric (ca. 32%), as shown in **Table ESI1**†. The larger porosity of the ribbon-like fibres may also relate to the elastic deformation[35]. This elastic behaviour is beneficial to air-filters as it can help to maintain the shape and porous structures against the external force or airflow.[36]

2.3 Morphology formation mechanisms

To understand the formation of the rod-zein fibre and ribbon-zein fibre by electrospinning as shown above, we propose the possible mechanisms as shown by Fig. 4a and b. For the zein-(AA/DI) system, it can be viewed as a stable solution which will maintain the solution state during evaporation. This happens because the boiling points of acetic acid and DI water are close to each other. As illustrated by Fig. 4a, the evaporation speed for the two solvents (AA and DI) is similar and the evaporation is a coordinated process. In other words, the ratio between AA and DI in the system won't change notably during the evaporation, which is critical to maintaining the solution state of the zein protein. This point can be proved by the digital photo in Fig. 4a, which shows no film formation on the solution surface during the evaporation. As a result, the electrospun fibre keeps a wet solution state and shrinks uniformly with the removal of the two solvents, resulting in a straight rod fibre as illustrated by Fig. 4a.

For the zein-(acetone/butanol/DI) system, it can be viewed as a unique metastable solution. This metastable solution will experience complicated phase transition during the evaporation as explained below and illustrated in Fig. 4b. Firstly, the mixture solvent is composed of components with very different boiling points. The boiling points for acetone, butanol and DI water are 56 ℃, 117 ℃ and 100 ℃ at standard atmospheric pressure, respectively. During the process of drying, the acetone will evaporate firstly due to its low boiling point. As a result, the compositions or ratios among the solvent components near the fibre surface will be very different from the original state. At the same time, the protein near the surface may precipitate out

and form a semi-solid shell on the surface. This point can be confirmed by two facts. Firstly, we study how the viscosity of the two solutions changes with the evaporation time in an open environment by a parallel dynamic rheometer. As shown by Fig. 4c and Fig. ESI3†, the viscosity of the stable zein solution increases with evaporation time steadily due to the change of zein concentration. In contrast, the viscosity of the metastable zein solution increases remarkably and reaches 1684 Pa·s in only ca. 400 s, which indicates a liquid-to-solid transition near the surface of the sample.[37] This phenomenon is also confirmed by the second digital photo in Fig. 4b, which shows a strong protein film formed on the solution surface after evaporation for ca. 30 min. The second fact is that the zein protein cannot be well dissolved in the mixture solvent with butanol and DI, or in any of the individual solvents as shown in Fig. 4d. This means the combination of the three solvent components is critical to dissolve the zein protein. In other words, removal of any component first from the mixture solvent will result in protein precipitation. This is exactly the reason why the zein-(acetone/butanol/DI) system has been referred as a metastable solution. Therefore, with uncoordinated evaporation of removing acetone fast and firstly, the fibre surface will experience a phase transition from liquid to solid or semi-solid. Meanwhile, the inside part of the fibre may maintain its solution state. With the further evaporation of the residual solvents (DI and butanol), there will be a volume shrinkage due to the solidification of the inside part of the fibre. During this process, the fibre may be compressed by air pressure and finally form a ribbon-like fibre as shown in Fig. 4b. The above phenomenon is very similar to the evacuation of a sealed soft tube filled with water. The above complicated evaporation and protein solidification should also be responsible for the self-curving of the ribbon-like fibre. One possible explanation is that the ribbon-like fibre experiences a non-uniform shrinkage during the solidification.

2.4 Air-filtration performance

The above studies on the unique ribbon-zein fabric not only bring about a significant finding on electrospinning technology, but also enable the fabrication of advanced filtration materials as shown below. The removal efficiencies for PM pollutants for the ribbon-zein fabric, rod-zein fabric and a commercial air-filter are compared in Fig. 5a and Fig. ESI5†. As shown, the ribbon-zein fabric

air-filter exhibits significantly higher removal efficiency (ca. 99.9%) than the rod-zein air-filter (ca. 76%) when the pressure drop for these two fabrics is fixed to be about 110 Pa (please see Fig. ESI4†). Instead of fixing pressure drop, one can also fix the areal density for the two types of zein fabrics and compare the performance. For example, if the areal density is fixed as about 12 g/m^2, the PM removal efficiencies are very close for these two types of zein fabrics. However, the ribbon-zein fabric shows a pressure drop of 107 Pa, which is only about 8% of the rod-zein fabric (ca. 1270 Pa, please see Fig. ESI4†). It is noted that the removal efficiencies of PM for the ribbon-zein air-filter are also higher than those by a commercial air-filter that shows a much higher pressure drop of 240 Pa and possesses a high areal density of 143.9 g m^{-2}. From this result, one can find that the ribbon-zein air-filter has significant advantages in filtration as compared with rod-type fabric and traditional polymeric fabric: it can give rise to much higher removal efficiencies for a broad range of PM with the same pressure drop as other filters, or it can realize the same filtration efficiencies with much lower pressure drop as compared with the counterparts. In a word, it combines two critical filtration properties: high filtration efficiency and low flow resistance.

The ribbon-zein fabric air-filter combines high filtration efficiency and low flow resistance at a high loading of active materials, which is the key to realize another critical filtration property, that is, high filtration capacity for long service life. For air-filter, life span is important for the practical applications.[26, 38] In this study, we investigate the long-term filtration performance for $PM_{1-2.5}$ for the ribbon-zein, rod-zein and commercial air-filters under the condition of a hazardous level ($PM_{2.5}$ concentration is above 300 μg m^{-3}) with an airflow speed of 4 L min^{-1}. The long-term testing results are compared in Fig. 5b. For the rod-zein fabric, the removal efficiency for $PM_{1-2.5}$ starts to drop after continuously filtering about 750 L highly polluted air. In contrast, the $PM_{1-2.5}$ removal efficiency for the ribbon-zein air-filter maintains its high value of 99.9% even after filtering about 1400 L highly polluted air. The filtration performance stability is also better than the commercial counterpart that showed a reduced removal efficiency of 98.88% after filtering about 1500 L highly polluted air. Moreover, the filtration capacity is highly dependent on the loading of active

materials. Therefore, keeping a low flow resistance with a high loading of active material is critical for high-capacity air-filters[9]. The dependence of pressure drop on the active material loading (i.e., areal density) for the two protein fabrics are compared in Fig. 5c. From this Fig., one can find that, firstly, the pressure drop of the two fabrics increases with the increasing of areal density. However, for the ribbon-zein air-filter, the pressure drop is much less sensitive to the increasing areal density as compared with that for the rod-zein air-filter. This is mainly due to the cotton-candy-like loose structures as illustrated in Fig. 1b. For example, even with a high areal density of 12 g m^{-2}, the pressure drop of the ribbon-zein air-filter is only 99 Pa. However, the pressure drop for the rod-zein air-filter reaches 1270 Pa with the same areal density. What's more, the pressure drop of the ribbon-zein air-filter is always much lower than the rod-zein air-filter with the same areal density. Hence, the filtration capacity of the ribbon-zein air-filter can be easily doubled by stacking two layers of the fabrics without notably increasing the pressure drop. This result indicates that the ribbon-zein fabric is a promising material for heavy duty filtration application.

The zein-protein fabrics can remove not only PM pollutants, but also toxic chemicals as shown in our previous studies.[26] In this study, we also inspect how the ribbon-zein contributes to the removal of toxic chemicals. We particularly investigate the removal efficiencies of formaldehyde (HCHO) and carbon monoxide (CO) for the ribbon-zein, rod-zein fabrics, as well as a commercial air-filter with activated carbon. As shown in Fig. 5d, both the ribbon-zein and rod-zein fabrics show removal efficiency about 81% for HCHO, which is similar to that for the commercial air-filter with activated carbon. For CO, the ribbon-zein fabric shows a little higher removal efficiency (37.5%) than the rod-zein fabric (33%). This value is even close to the commercial air-filter (ca. 39%) combined with considerable activated carbon. The unique molecular structures and the functional groups from different types of amino acids play critical roles in capturing small chemical molecules.[4, 6, 18, 24, 27] More interestingly, the above result indicates that the unique ribbon-type fibre also promotes the trapping capability for chemical gaseous molecules. In short, the ribbon-zein air-filter is a multi-functional filtration material that shows better chemical filtration performances as compared with the rod-zein air-filter. It

realizes a similar chemical filtration performance with the commercial one combined with activated carbon, but a much lower flow resistance and better PM filtration performance.

The morphology of the two types of zein air-filters is further studied after the long-term testing as introduced above. As shown in Fig. 6a, d and g, j, the notable colour change of the air-filter from white to yellow after filtration is an obvious indication for adsorption of pollutants. The SEM images of the morphology before and after filtration are shown in Fig. 6b-c, e-f, h-i, k-l and Fig. ESI6-8†, for the two types of zein fabric air-filters. More specifically, one can clearly observe that numerous small particulate pollutants, which are much smaller than the pore size of the fabrics, are tightly trapped by the zein protein fabric. After the long-term filtration testing, there is even a pollutant coating layer formed on the fibre surface. These SEM images indicate that the air pollutants can be adsorbed on the surface of the zein fibres and there are strong interactions between the zein fibres and various pollutants. However, as shown in Fig. 6e, k and Fig. ESI6-8†, there is a big difference in morphology between the rod-zein filter and ribbon-zein filter. More specifically, for the rod-zein fabric filter, one can observe film formation among different fibres, which is due to the accumulation of pollutants after the long-term testing. In contrast, for the ribbon-zein fabric filter, there is no film formation and no obvious morphology change after the long-term filtration testing. A closer observation of the ribbon-zein fibre after the testing reveals that the pollutants are trapped and stored in a local “reservoir” formed by the curved ribbon-like fibre. The above big difference in morphology after filtration testing has a significant effect on the air-flow resistance. As shown in Fig. 6m, the pressure drop for the rod-zein air-filter increased by ca. 110 Pa after filtration, which is clearly due to the film formation as shown by the SEM image in Fig. 6e and Fig. ESI7†. However, for the ribbon-zein air-filter, there is almost no change in pressure drop even after the long-term testing. This result further indicates that the cotton-candy-like loose structure is a big advantage for high-capacity filter to keep a low flow resistance even during long-term service.

The above filtration studies have well proved the hypothesis proposed in Fig. 1. The unique morphology of the self-curved ribbon-like fibres is the key to achieve low

pressure drop, high removal efficiencies, high filtration capacity and good stability in flow resistance. The advantage in filtration performance can be further proved by the quality factor (QF) of air-filters, which takes both removal efficiency and pressure drop into consideration.[9, 24, 39] The QF results are shown in Table ESI1†. In particular, the QF of ribbon-zein air-filter is 0.075, much higher than 0.014 for the rod-zein air-filter for $PM_{2.5}$ removal. A higher QF value means the filter can remove pollutants with high efficiency but a low pressure drop, which is highly desired by high-performance air-filters. Considering the fact that the fabric filters are usually prepared with different amount of active materials, a normalized pressure drop (ΔP_n) is defined as below to better compare the flow-resistant property of air-filters:

$$\Delta P_n = \Delta P/m \quad (1)$$

where ΔP is the pressure drop with a unit of Pa, m is the mass of active filtration materials with a unit of g. Therefore, the normalized pressure drop, ΔP_n, will take the unit of Pa g^{-1}, which removes the effect of mass on the pressure drop.[25] With this ΔP_n, the advantage in flow-resistant property is very obvious for the ribbon-zein air-filter. In particular, the ΔP_n is 4.148 KPa g^{-1}, much lower than 17.166 KPa g^{-1} for the rod-zein air-filter (see Table ESI1†). This normalized pressure drop is mainly dependent on the porous structures of the fabrics, which can well reflect the advantage of cotton-candy-like loose structures for filtration application.

3. Experimental Section

3.1 Materials. Zein from corn (95 % purity) was purchased from Sigma-Aldrich Co., Ltd. 1-Butanol (99% purity), Acetic acid (99.9% purity), Acetone were purchased from Fisher Chemical, EMO Millipore, KOPTEC and MACRON Co., Ltd. All materials and solvents were used without further purification.

3.2 Preparation of Zein solutions. To prepare the traditional stable zein solution, zein powders were dissolved in a mixture solvent of acetic acid (AA) and distilled water (DI) with a weight ratio of 4:1.[6, 26] After about 30 minutes of stirring, a homogeneous yellow solution with denatured zein was achieved. The solid concentration was 25 wt%, which was fixed for all the zein solutions if not specified below. To prepare the metastable zein solution, zein powders were dissolved in

a special mixture solvent composed of acetone, 1-butanol and DI with a weight ratio of 2:1:1. All the solutions were treated by sonication in water bath at room temperature, and then set down for at least 2 hours before electrospinning, in order to remove the air bubbles. The reason we refer the first zein solution in AA/DI as a stable solution is that AA and DI have similar boiling points, which helps to maintain the AA/DI ratio for the solvent during evaporation, and thereof the dissolving of zein. In contrast, for the metastable zein solution, the solvent is composed of three components (butanol, DI and acetone) with very different boiling points. It is found that any combination of two from these three components cannot effectively dissolve zein. This fact indicates that the zein solution in this three-component solvent is a metastable solution. In other words, the solution will become unstable if one of the three components in the solvent evaporates much faster than the other two. At this point, the acetone with boiling point of 56 °C is the key for preparation of the metastable solution.

3.3 Fabrication of Zein fabrics by electrospinning. The above zein solutions were loaded in a syringe (Monojet Kendall) with a 21-gauge blunt-tip needle. A high-voltage power source (ES50P-5W, Gamma High Voltage Research) controlled the voltage for electrospinning: 16 kV for the metastable zein solution, 18 kV for the stable zein solution. Zein solution was pumped by A mono inject syringe pump (KD Scientific, KDS-100). Paper towel substrate was fixed on a grounded metal plate to collect the zein-fibres onto the paper towel. The distance from the needle to the paper towel was fixed at 14 cm. The flow rates of the metastable zein solution and stable zein solution were 2.5 mL h^{-1} and 1 mL h^{-1}, respectively. Moreover, the vertical and horizontal location of the needle was adjusted constantly to achieve a unique fabric with a controlled fibre diameter, thickness and areal density.[26]

3.4 Characterization of zein solutions. The nano-particles of the metastable and stable zein solutions were determined by a dynamic laser light scattering (Zetasizer Nano, Malvern Instruments).[40] The viscosity of the metastable and stable zein solutions was determined by a hybrid rheometer (DISCOVERT, HR-2). The transmittance of the metastable and stable zein solutions

was scaned in the range of 200-1100 nm using a Lambda 25 UV/VIS Spectrometer (PerkinElmer).

3.5 Characterization of zein fabrics. Fourier transform infrared (FTIR, Thermofisher iS10) spectrophotometer was used to investigate the functional groups of zein fabrics. The morphological characteristics of the rod and ribbon-zein fabrics were investigated by scanning electron microscopy (SEM, FEI SEM Quanta 200F) and transmission electron microscope (TEM, FEI TEM T20). The mechanical properties of the rod and ribbon-zein fabrics were tested by a universal testing machine (Instron, 5565A) with a tensile rate of 5 mm min^{-1}.[26] The porosity was determined via equation (2):

$$\Phi = V_V/V_T \quad (2)$$

where V_V is the volume of void-space (silicone oil) and V_T is the total volume of air-filter.

3.6 Air-Filtration Testing. The PM with particle sizes ranging from 0.01 to 10 μm and toxic gases (HCHO and CO) were produced by burning incense. The concentrations of PM and toxic chemicals (HCHO and CO) were diluted in a glass bottle to the level that was measured by a particle counter (CEM, DT-9881) with chemical sensors for HCHO and CO. The airflow rate was fixed as 4 cm s^{-1} to test the filtration performance and the pressure drop by a manometer (UEi, EM201-B). Air-filtration testing was performed on a circular air-filter sample with a diameter of 37 mm, which was placed and sealed in a homemade sample holder.[4, 26, 27]

The removal efficiency (η) of pollutants (PM, HCHO and CO) was determined via equation (3):

$$\eta = (C_p\text{-}C_c)/C_p \quad (3)$$

where C_p and C_c are the air pollutant concentration before and after filtration testing, respecitively.[41]

The quality factor (QF) was determined via equation (4):

$$QF = -\ln(1\text{-}\eta)/\Delta P \quad (4)$$

Where ΔP is the pressure drop of the air-filter.[26]

4. Conclusions

In summary, via studies of electrospun protein fibres from a unique metastable solution, we have demonstrated a multi-functional protein fabric with cotton-candy-like loose structures made of ribbon-like fibres for advanced and sustainable air filtration application. Different from traditional electrospun rod-

type fibres forming a compact fabric structure, electrospinning the metastable protein solution produces the unique self-curved ribbon-like fibres and cotton-candy-like loose fabrics. This ribbon protein fabric has shown significant performances in airflow resistance, removal efficiencies, filtration capacity and stability of pressure drop during long-term filtration. This study does not only provide a facile electrospinning strategy for fabrication of multi-functional loose ribbon-like fibres, but also suggests a guideline for the design of filter materials with special morphology leading to advanced performances for air filtration application and beyond.

Conflicts of interest

There are no conflicts to declare.

Acknowledgements

This work was supported by the National Natural Science Foundation of China (31571847), Science and Technology Innovation Program of Hubei (2015ABA035) and supported partially by USDA NIFA 201567021-22911 and NSF CMMI 1463616. The authors appreciate the School of Biological Sciences Franceschi Microscopy & Imaging Center (FMIC), Washington State University for providing the field emission electron microscope.

Notes and references

1. J. Li, M. Li, F. Shen, Z. Zou, M. Yao and C.-y. Wu, *Environmental science & technology*, 2013, **47**, 10660-10666.
2. S. Weon, E. Choi, H. Kim, J. Y. Kim, H.-J. Park, S.-m. Kim, W. Kim and W. Choi, *Environmental science & technology*, 2018.
3. S. Zhang, J. Sun, D. Hu, C. Xiao, Q. Zhuo, J. Wang, C. Qin and L. Dai, *Journal of Materials Chemistry A*, 2018.
4. H. Souzandeh, L. Scudiero, Y. Wang and W.-H. Zhong, *ACS Sustainable Chemistry & Engineering*, 2017.
5. R. Zhang, C. Liu, P.-C. Hsu, C. Zhang, N. Liu, J. Zhang, H. R. Lee, Y. Lu, Y. Qiu and S. Chu, *Nano letters*, 2016, **16**, 3642-3649.
6. H. Souzandeh, B. Molki, M. Zheng, H. Beyenal, L. Scudiero, Y. Wang and W.-H. Zhong, *ACS applied materials & interfaces*, 2017, **9**, 22846-22855.
7. S. Platt, I. E. Haddad, S. Pieber, R.-J. Huang, A. Zardini, M. Clairotte, R. Suarez-Bertoa, P. Barmet, L. Pfaffenberger and R. Wolf, *Nature communications*, 2014, **5**, 3749.
8. X. Han and L. P. Naeher, *Environment international*, 2006, **32**, 106-120.
9. C. Liu, P.-C. Hsu, H.-W. Lee, M. Ye, G. Zheng, N. Liu, W. Li and Y. Cui, *Nature communications*, 2015, **6**, 6205.
10. M. M. Maricq, *Journal of Aerosol Science*, 2007, **38**, 1079-1118.
11. E. M. Dunne, H. Gordon, A. Kürten, J. Almeida, J. Duplissy, C. Williamson, I. K. Ortega, K. J. Pringle, A. Adamov and U. Baltensperger, *Science*, 2016, **354**, 1119-1124.
12. L. Yao, O. Garmash, F. Bianchi, J. Zheng, C. Yan, J. Kontkanen, H. Junninen, S. B. Mazon, M. Ehn and P. Paasonen, *Science*, 2018, **361**, 278-281.
13. J. E. Sordillo, K. M. Switkowski, B. A. Coull, J. Schwartz, I. Kloog, H. Gibson, A. A. Litonjua, J. Bobb, P. Koutrakis and S. L. Rifas-Shiman, *Scientific reports*, 2018, **8**.
14. N. Mahowald, *Science*, 2011, **334**, 794-796.
15. A. Nel, *Science*, 2005, **308**, 804-806.
16. Y. Zhang, G.-Q. Zang, Z.-H. Tang, X.-H. Chen and Y.-S. Yu, *American journal of infection control*, 2014, **42**, 815.
17. E. Dauber, *Journal*, 2002.
18. H. Souzandeh, K. S. Johnson, Y. Wang, K. Bhamidipaty and W.-H. Zhong, *ACS applied materials & interfaces*, 2016, **8**, 20023-20031.
19. P. Li, C. Wang, Y. Zhang and F. Wei, *Small*, 2014, **10**, 4543-4561.
20. Z. Dai, J. Su, X. Zhu, K. Xu, J. Zhu, C. Huang and Q. Ke, *Journal of Materials Chemistry A*, 2018.
21. J. Xu, C. Liu, P.-C. Hsu, K. Liu, R. Zhang, Y. Liu and Y. Cui, *Nano letters*, 2016, **16**, 1270-1275.
22. Y. Bian, R. Wang, S. Wang, C. Yao, W. Ren, C. Chen and L. Zhang, *Journal of Materials Chemistry A*, 2018.
23. B. Zhang, Z.-G. Zhang, X. Yan, X.-X. Wang, H. Zhao, J. Guo, J.-Y. Feng and Y.-Z. Long, *Nanoscale*, 2017, **9**, 4154-4161.
24. C. Wang, S. Wu, M. Jian, J. Xie, L. Xu, X. Yang, Q. Zheng and Y. Zhang, *Nano Research*, 2016, **9**, 2590-2597.
25. X. Fan, Y. Wang, L. Kong, X. Fu, M. Zheng, T. Liu, W.-H. Zhong and S. Pan, *ACS Sustainable Chemistry & Engineering*, 2018.

26. H. Tian, X. Fu, M. Zheng, Y. Wang, Y. Li, A. Xiang and W.-H. Zhong, *Nano Research*, 1-13.
27. H. Souzandeh, Y. Wang and W.-H. Zhong, *RSC Advances*, 2016, **6**, 105948-105956.
28. Y. Zhao, M. He, L. Zhao, S. Wang, Y. Li, L. Gan, M. Li, L. Xu, P. R. Chang and D. P. Anderson, *ACS applied materials & interfaces*, 2016, **8**, 2781-2795.
29. V. Gilbert, M. Rouabhia, H. Wang, A.-L. Arnould, G. Remondetto and M. Subirade, *Biomaterials*, 2005, **26**, 7471-7480.
30. Y. Li, Y. Jiang, F. Liu, F. Ren, G. Zhao and X. Leng, *Food Hydrocolloids*, 2011, **25**, 1098-1104.
31. S. Ovchinnikov, H. Park, N. Varghese, P.-S. Huang, G. A. Pavlopoulos, D. E. Kim, H. Kamisetty, N. C. Kyrpides and D. Baker, *Science*, 2017, **355**, 294-298.
32. J.-E. Shea and C. L. Brooks III, *Annual review of physical chemistry*, 2001, **52**, 499-535.
33. C. M. Dobson, *Nature*, 2003, **426**, 884.
34. C. E. Ophardt, *Virtual Chembook. Elmhurst College*, 2003.
35. D. Lacerda, F. Ptak and R. Prioli, *MRS Advances*, 2018, 1-6.
36. M. Li, Y. Feng, K. Wang, W. F. Yong, L. Yu and T.-S. Chung, *Environmental Science & Technology*, 2017, **51**, 10041-10049.
37. H. Zhang, S. Xi, Y. Han, L. Liu, B. Dong, Z. Zhang, Q. Chen, W. Min, Q. Huang and Y. Li, *Soft matter*, 2018, **14**, 3455-3462.
38. B. Shi and L. Ekberg, *Environmental science & technology*, 2015, **49**, 6891-6898.
39. Y. Cheng, C. Wang, J. Zhong, S. Lin, Y. Xiao, Q. Zhong, H. Jiang, N. Wu, W. Li and S. Chen, *Nano Energy*, 2017, **34**, 562-569.
40. S. Patil, A. Sandberg, E. Heckert, W. Self and S. Seal, *Biomaterials*, 2007, **28**, 4600-4607.
41. C. Liu, P.-C. Hsu, H.-W. Lee, M. Ye, G. Zheng, N. Liu, W. Li and Y. Cui, *Nature communications*, 2015, **6**, 6205.

Journal of Materials Chemistry A

ARTICLE

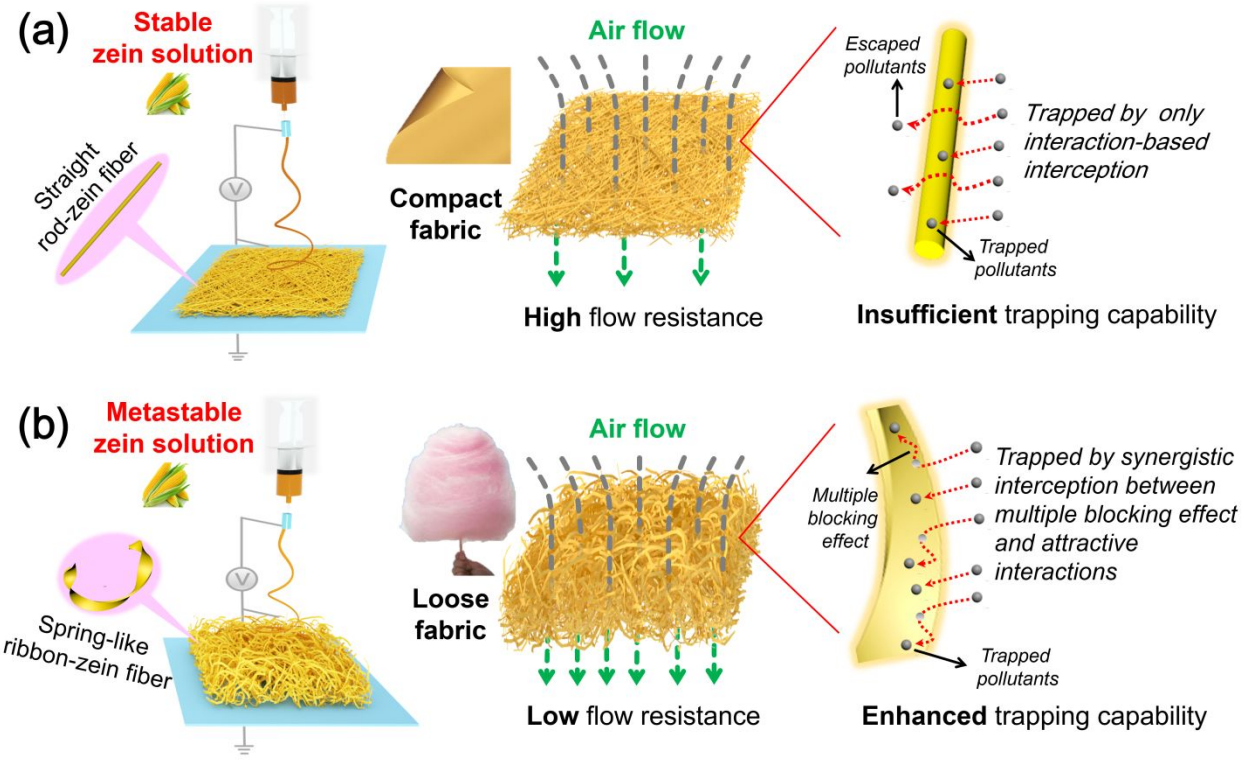

Fig. 1. **Schematic of fabrics by electrospinning different types of zein solution for air-filtration**: (a) traditional stable solution giving rise to straight rod-zein fibres and compact fabric; (b) metastable solution generating self-curved ribbon-zein fibres and cotton-candy-like loose fabric. The differences for the two types of zein fabrics in flow resistance and trapping capability of air pollutants are illustrated as well (For details, see the text).

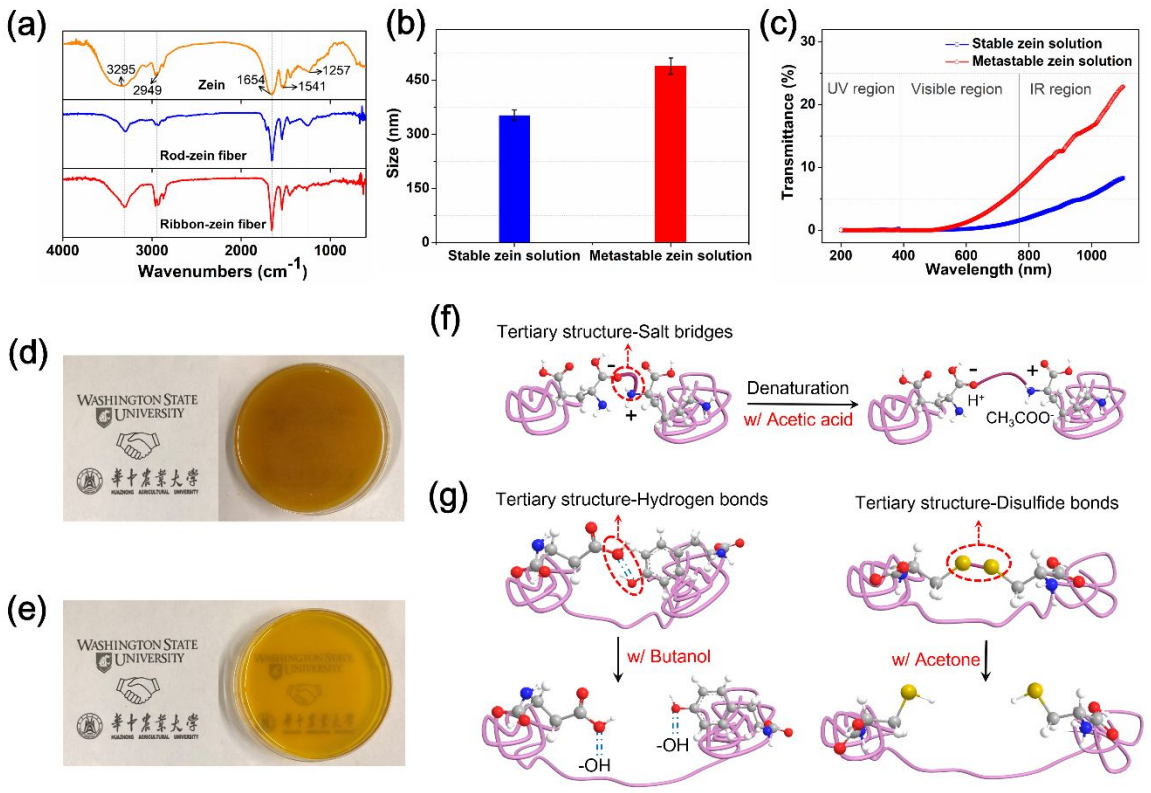

Fig. 2. Denaturation of zein in AA/DI (stable solution) and acetone/butanol/DI (metastable solution) mixture solvents. (a) FTIR spectra of pristine zein, rod-zein and ribbon-zein fabric prepared by the two mixture solvent systems; (b) Particle size of the stable and metastable zein solutions; (c) Transmittance spectra of the stable and metastable zein solutions in the range of 200-1100 nm; (d) and (e), Digital photos of transmittance of the stable and metastable zein solutions, respectively; (f) and (g), Illustration of the denaturation of zein by the help of acetic acid and butanol/acetone in the stable and metastable solutions, respectively.

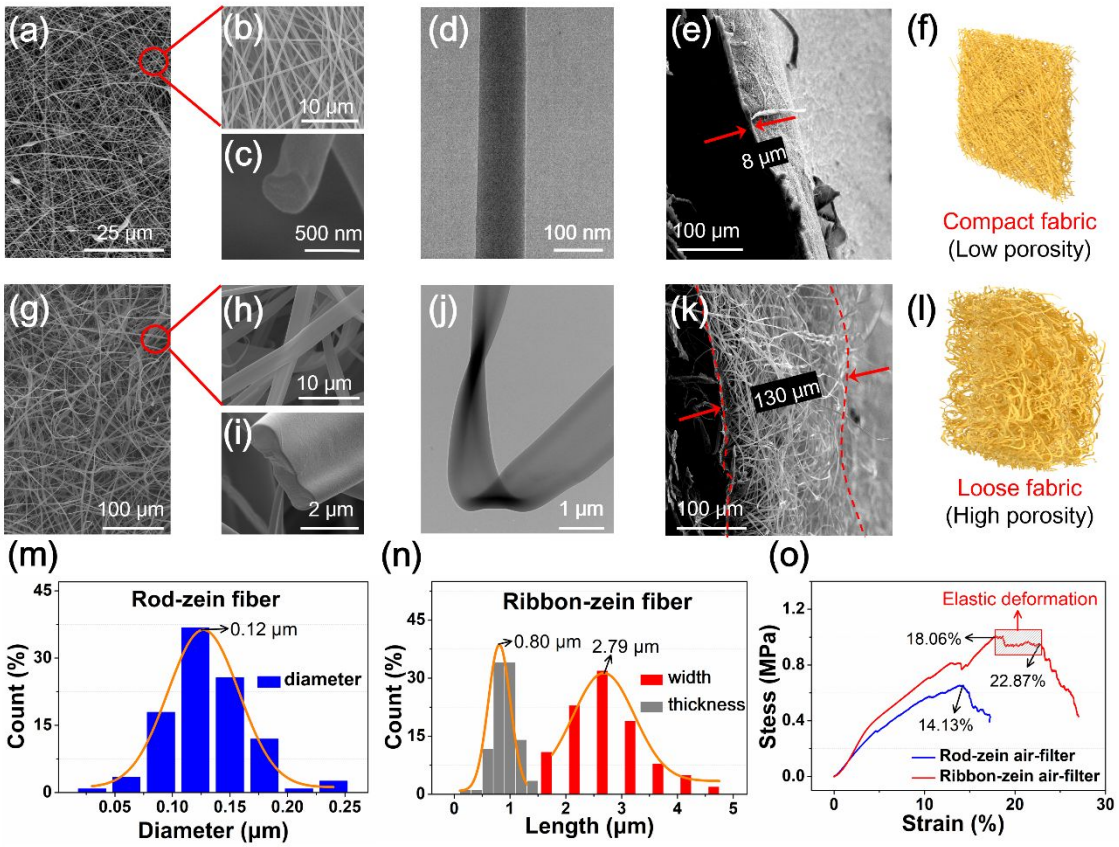

Fig. 3. Rod-zein and ribbon-zein fabrics based on the stable and metastable protein solutions. (a) - (d), SEM and TEM images of the rod-zein fibres by electrospinning of the stable zein solution in AA/DI, (e) SEM image of the cross-section of the rod-zein fabric; (f) Schematic of the fabric structures with the rod-zein fibres; (g) - (j), SEM and TEM images of the self-curved ribbon-zein fibre by electrospinning of the metastable zein solution in acetone/butanol/DI, (k), SEM image of the cross-section of the ribbon-zein fabric, (l) Schematic of the fabric structures with the ribbon-zein fibres; (m) The diameter distribution for the rod-zein nanofibers; (n) The distribution of width and thickness of the ribbon-zein fibres; (o) Comparison of stress-strain curves for the rod-zein and ribbon-zein fabrics.

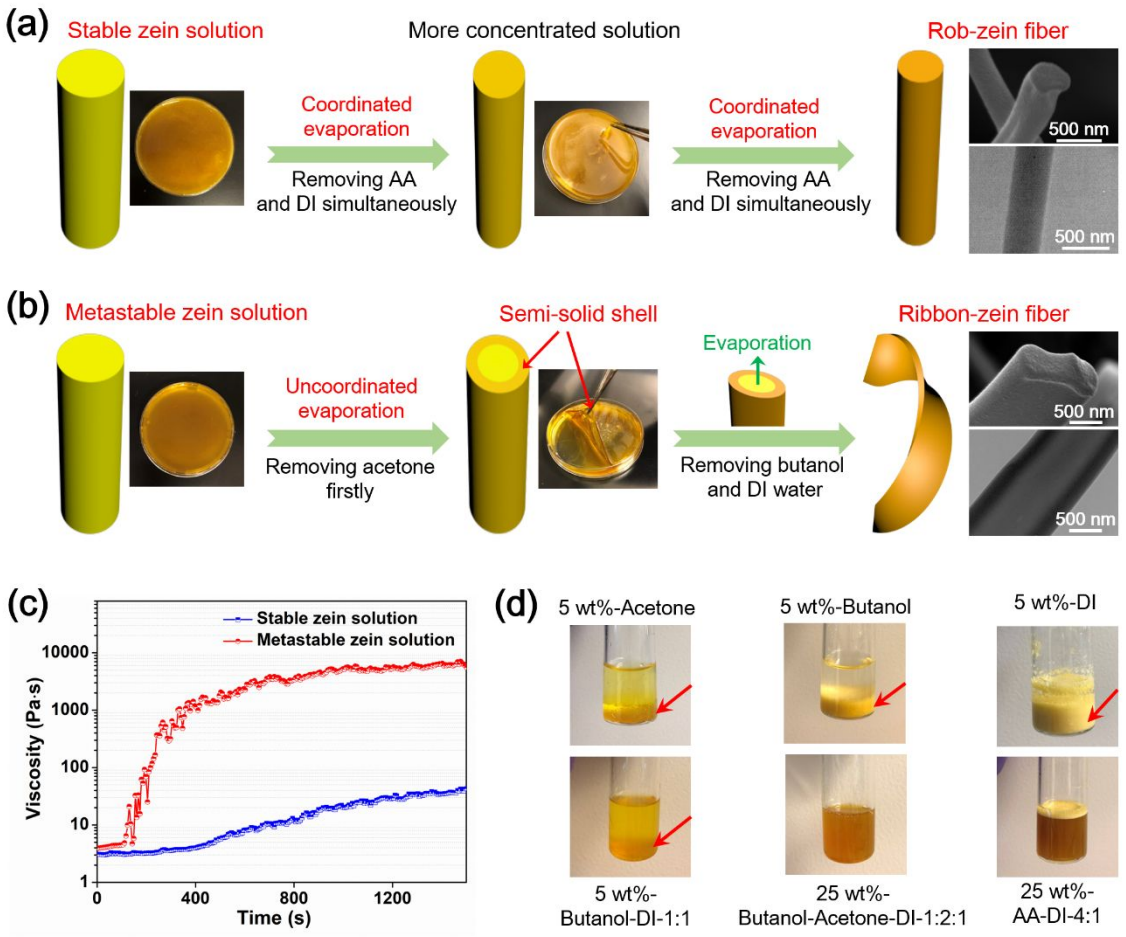

Fig. 4. The formation mechanisms of rod-zein and ribbon-zein fibres by electrospinning. (a) Rod-zein fibre from stable protein solution; (b) Ribbon-zein fibre from metastable solution; (c) Viscosity *vs.* evaporation time for the stable and metastable zein solutions; (d), Digital photos showing the zein solubility in acetone, butanol, DI water, butanol-DI, butanol-acetone-DI and AA-DI solvents.

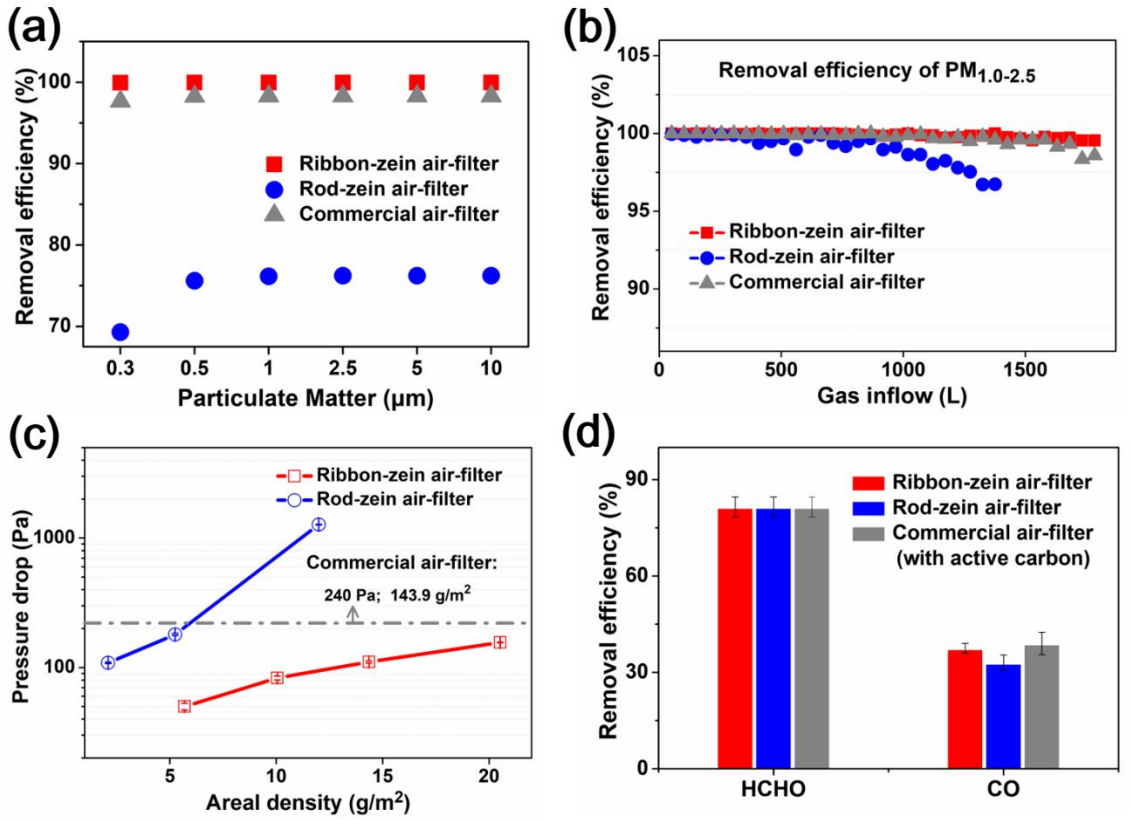

Fig. 5. Air filtration performance. (a) The PM removal efficiencies for the ribbon-zein, rod-zein and a commercial air-filter; (b) Comparison of the long term performance for $PM_{1.0-2.5}$ removal; (c) The dependence of pressure drop on areal density for the ribbon-zein and rod-zein fabrics (the dashed line represents a commercial air-filter); (d) Chemical removal efficiency for formaldehyde (HCHO) and carbon monoxide (CO) by the ribbon-zein, rod-zein fabrics and the commercial air-filter with activated carbon.

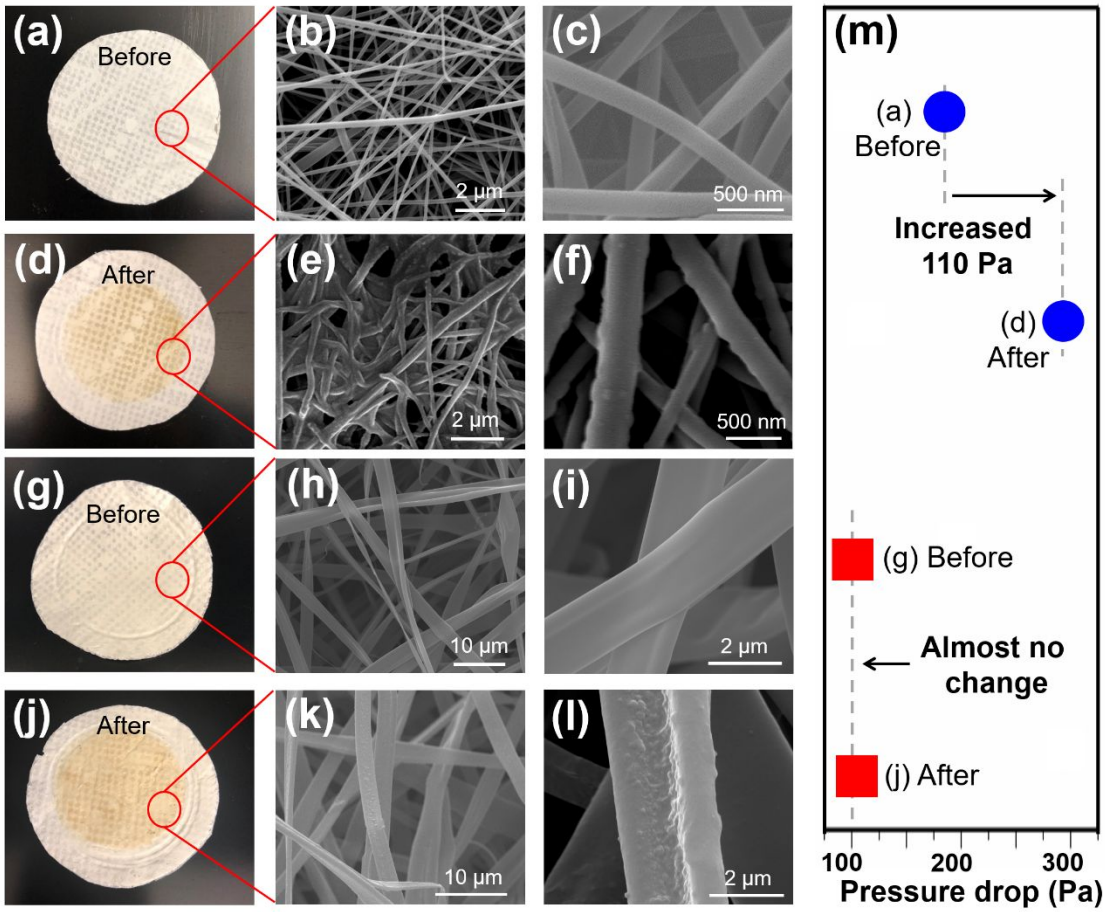

Fig. 6. Fabric morphology and pressure drop after long-term filtration. (a) Digital photo of rod-zein air-filter before filtration testing; (b-c) SEM images of rod-zein air-filter before filtration; (d) Digital photo of rod-zein air-filter after filtration testing; (e-f) SEM images of rod-zein air-filter after filtration; (g) and (j) Digital photos of ribbon-zein air-filter before and after filtration testing, respectively; (h-i) and (k-l) SEM image of ribbon-zein air-filter before and after filtration, respectively; (m) The pressure drop of rod-zein air-filter and ribbon-zein air-filter before and after filtration.

TOC Figure

A cotton-candy inspired, multi-functional protein fabric with novel ribbon-like fiber morphology is proposed for advanced and sustainable filtration application.